JACS
JOURNAL OF THE AMERICAN CHEMICAL SOCIETY
Communication
pubs.acs.org/JACS

Highly Reproducible Perovskite Solar Cells with Average Efficiency of 18.3% and Best Efficiency of 19.7% Fabricated via Lewis Base Adduct of Lead(II) Iodide

Namyoung Ahn,[†,§] Dae-Yong Son,[‡,§] In-Hyuk Jang,[‡] Seong Min Kang,[†] Mansoo Choi,*[,†] and Nam-Gyu Park*[,‡]

[†]Department of Mechanical and Aerospace Engineering, Seoul National University, Seoul 151-742, Korea
[‡]School of Chemical Engineering and Department of Energy Science, Sungkyunkwan University, Suwon 440-746, Korea

Supporting Information

ABSTRACT: High efficiency perovskite solar cells were fabricated reproducibly via Lewis base adduct of lead(II) iodide. PbI_2 was dissolved in *N*,*N*-dimethyformamide with equimolar *N*,*N*-dimethyl sulfoxide (DMSO) and CH_3NH_3I. Stretching vibration of S═O appeared at 1045 cm^{-1} for bare DMSO, which was shifted to 1020 and 1015 cm^{-1} upon reacting DMSO with PbI_2 and PbI_2 + CH_3NH_3I, respectively, indicative of forming the adduct of PbI_2·DMSO and CH_3NH_3I·PbI_2·DMSO due to interaction between Lewis base DMSO and/or iodide (I^-) and Lewis acid PbI_2. Spin-coating of a DMF solution containing PbI_2, CH_3NH_3I, and DMSO (1:1:1 mol %) formed a transparent adduct film, which was converted to a dark brown film upon heating at low temperature of 65 °C for 1 min due to removal of the volatile DMSO from the adduct. The adduct-induced $CH_3NH_3PbI_3$ exhibited high charge extraction characteristics with hole mobility as high as 3.9 × 10^{-3} $cm^2/(V\ s)$ and slow recombination rate. Average power conversion efficiency (PCE) of 18.3% was achieved from 41 cells and the best PCE of 19.7% was attained via adduct approach.

Since the report on the 9.7% solid-state perovskite solar cell employing $MAPbI_3$ (MA = CH_3NH_3) and spiro-MeOTAD in 2012,[1] overcoming the dissolution problem of $MAPbI_3$ in liquid electrolyte observed in the two important pioneer works in 2009 and 2011,[2,3] there is a surge in perovskite solar cell researches due to facile fabrication procedure and superb photovoltaic performance in both mesoscopic structure and planar structure.[4−7] As a result, a power conversion efficiency (PCE) of 20.1% was certified by national renewable energy laboratory.[8]

$MAPbI_3$ layer for perovskite solar cell can be prepared using either one-step coating[2,3] or sequential two-step coating.[9,10] It was reported that photovoltaic performance of devices prepared by two-step coating was superior to one-step method.[11] Recently solvent engineering method was proposed in one-step spin coating,[12] where DMSO was used as a cosolvent in the gamma-butyrolactone (GBL) solution containing MAI and PbI_2. One-step coated film was washed with toluene while spinning to get rid of solvent and to form a so-called intermediate phase of MAI-PbI_2-DMSO, by which an average PCE of about 15% together with a best PCE of 16.46% was achieved. However, the intermediate phase could not be identified by X-ray diffraction. Moreover, since toluene can wash not only GBL but also DMSO, it may be hard to induce a well-defined intermediate phase for reproducible and uniform growth of $MAPbI_3$.

Here we report highly reproducible perovskite solar cell via Lewis base adduct of PbI_2. Oxygen bearing Lewis base and/or iodide anion form adduct with Lewis acid PbI_2, which is evidenced by infrared spectroscopy. By utilizing volatile characteristics of Lewis base in adduct, a reproducible and facile process is developed, which eventually results in an average PCE of 18.3% from 41 cells and a best PCE of 19.7%.

Figure 1 shows schematic representation of the fabrication processes that we have studied. DMF solutions (50 wt %) containing MAI and PbI_2 (1:1 mol %) and MAI, PbI_2, and DMSO (1:1:1 mol %) are prepared. One-step spin coating at 4000 rpm leads to the rod shaped $MAPbI_3$ crystals that are not

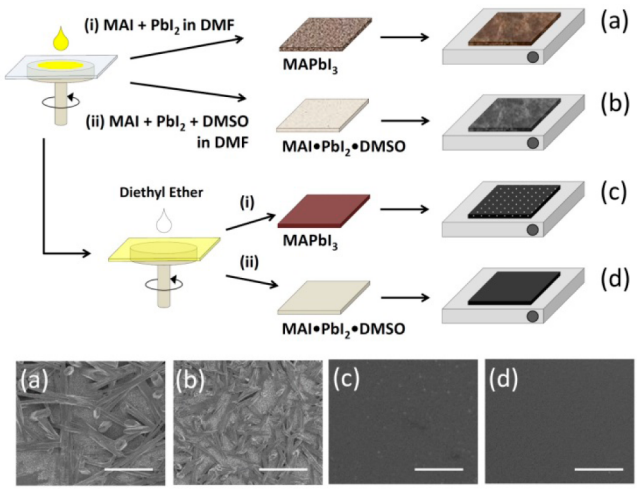

Figure 1. Schematic representation of fabrication procedure and plane-view scanning electron microscopy (SEM) images for the $MAPbI_3$ perovskite layers obtained by direct one-step spin-coating of the DMF solution containing (a) MAI and PbI_2 or (b) MAI, PbI_2, and DMSO. Panels (c) and (d) were prepared by same solution as that in panels (a) and (b), but diethyl ether was dripped during the film spinning.

Received: May 16, 2015
Published: June 30, 2015

DOI: 10.1021/jacs.5b04930
J. Am. Chem. Soc. 2015, 137, 8696−8699

fully covered on the substrate as observed in SEM images (Figure 1a,b), which is ascribed to different solubility of PbI_2 and MAI. The poor morphology is likely to be induced by difference in crystal growth rate between low solubility PbI_2 and high solubility MAI, while DMF is rapidly evaporating. However, highly densified $MAPbI_3$ films are formed when the solvent DMF is selectively washed with nonpolar diethyl ether while spinning because rapid evaporation problem may be solved by washing. As can be seen in SEM images in Figure 1c,d, both solutions produce smooth and homogeneous $MAPbI_3$ films, but the solution without DMSO leads to pinholes. This indicates that evaporation rate of DMF cannot be perfectly controlled by washing with diethyl ether. Surprisingly, DMSO-contained solution results in the pinhole-free film (Figure 1d), which indicates that crystal growth is highly regulated possibly due to adduct MAI·PbI_2·DMSO.

The dark brown $MAPbI_3$ film shown in Figure 2b is obtained by heating the transparent film (Figure 2a) observed right after

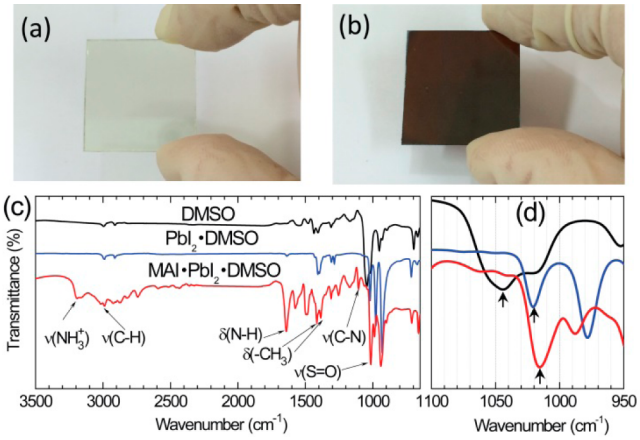

Figure 2. Photos of $MAPbI_3$ on FTO glass (a) before and (b) after annealing at 65 °C for 1 min and at 100 °C for 2 min. Fourier transform infrared spectrometer (FTIR) of (c) DMSO (solution), PbI_2·DMSO (powder), MAI·PbI_2·DMSO (powder), and (d) expanded the fingerprint region for the S═O vibrations.

washing the spin-coated MAI·PbI_2·DMSO layer with diethyl ether. The transparent film is indicative of adduct of PbI_2 with Lewis base DMSO and iodide in MAI. Lewis acid PbI_2 was known to form adduct by reaction with oxygen, nitrogen, and sulfur bearing Lewis bases, where lone pair electrons on oxygen in DMSO donates to Lewis acid Pb^{2+} in PbI_2 to form adducts with ratio of PbI_2/DMSO = 1:1 and 1:2.[13] Other solvents with oxygen donor such as *N*,*N*-dimethylacetamide (DMA) and DMF can form adduct with PbI_2, but more stable adduct is expected from DMSO due to stronger polarity (relative polarity of 0.444 for DMSO vs 0.386 for DMF[14]). Iodide (I^-) in MAI is also a strong donor and thereby readily forms adduct with PbI_2. It is actually observed that solubility of PbI_2 is more enhanced in the presence of MAI compared to the solubility of PbI_2 dissolved only in DMF, which indicates that I^- interacts strongly with PbI_2.

IR spectroscopic study is conducted to investigate adduct formation. Figure 2c shows IR spectra for liquid DMSO, powdered PbI_2·DMSO, and MAI·PbI_2·DMSO (see experimental for details). Stretching vibration of S═O (ν(S═O)) appears at 1045 cm^{-1} for the bare DMSO,[15] which is shifted to 1020 cm^{-1} for PbI_2·DMSO and further shifted to lower wavenumber of 1015 cm^{-1} for MAI·PbI_2·DMSO (Figure 2d and Table 1). The ν(S═O) at 1020 cm^{-1} is well consistent with the frequency of

Table 1. Stretching Frequency of S═O for Liquid DMSO and Powdered PbI_2·DMSO and MAI·PbI_2·DMSO Adducts, along with Their Chemical Structures

		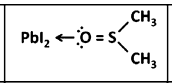	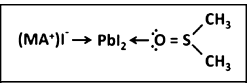
	DMSO	PbI_2•DMSO	MAI•PbI_2•DMSO
ν(S=O)	1045 cm^{-1}	1020 cm^{-1}	1015 cm^{-1}

1022 cm^{-1} observed for the 1:1 adduct of PbI_2·DMSO.[13] According to harmonic motion for diatomic model,[16] frequency of vibration is proportional to square root of force constant. Thus, the decreased S═O stretching frequency indicates that force constant is decreased, which is due to decrease in bond strength between sulfur and oxygen as a consequence of the adduct formation. Thus, the S═O stretching frequencies of PbI_2·DMSO and MAI·PbI_2·DMSO are detected in lower wavenumber than that of DMSO. It is noted that the S═O stretching wavenumber for MAI·PbI_2·DMSO is lower than that of PbI_2·DMSO. The S═O bond strength is expected to be more decreased when more Lewis acids are interacted with DMSO.[13] NH_3^+ stretching peak appears in MAI·PbI_2·DMSO (Figure 2c), from which the S═O bond strength is further decreased due to more interaction with Lewis acids of MA^+ and Pb^{2+} ions.

Adduct of PbI_2 with DMSO and MAI is confirmed, as evidence by IR spectroscopic study. Thus, the transparent film in Figure 2a represents the adduct MAI·PbI_2·DMSO. Regarding the washing solvent, since toluene and chlorobenzene are miscible with DMSO,[12,17] we have found that diethyl ether is a more proper solvent to keep the nominal ratio of MAI/PbI_2/DMSO = 1:1:1 because it dissolves only DMF and thereby leads to well-defined adduct. Since DMSO in adduct is known to be volatile,[13] the transparent film can be changed to brown $MAPbI_3$ upon blowing or being exposing to air for a few hours. It was observed that the colorless transparent needle crystal obtained from the saturated solution of DMSO with PbI_2 recovered original yellow color in air due to volatility of DMSO.[18] However, the resulting $MAPbI_3$ film is found to be inhomogeneous because vaporization of DMSO occurs gradually from the surface of the adduct film. We have found that low temperature heat treatment at 65 °C for 1 min is effective and sufficient to remove entire DMSO from the adduct. Highly dense and homogeneous $MAPbI_3$ films are eventually obtained by further annealing at 100 °C for 2 min. It is noted that equimolar DMSO plays an important role to form high quality perovskite films since excess DMSO such as PbI_2·MAI·DMSO (1:1:2 mol %) precursor results in extra PbI_2 upon exposing in air (Figure S1). The adduct-induced $MAPbI_3$ is found to be quite stable in air atmosphere (Figure S2).

The charge carrier transport property of the $MAPbI_3$ prepared via adduct is studied by photoinduced charge extraction by linearly increasing voltage (photo-CELIV)[19] with FTO/bl-Al_2O_3/mp-TiO_2/$MAPbI_3$/spiro-MeOTAD/Ag configuration (bl and mp stand for blocking and mesoporous). Figure 3 shows the current transient of photo-CELIV for the $MAPbI_3$ layers prepared via adduct of MAI·PbI_2·DMSO, which is compared with the $MAPbI_3$ prepared by spin-coating of the DMF solution without DMSO and washing with diethyl ether. Charge carrier mobility is calculated from the current (j)−time (t) curve in Figure 3a. A charge extraction CELIV peak appears at 3 μs after applying triangular increasing voltage ramp, and then current is saturated to the displacement current of the

DOI: 10.1021/jacs.5b04930
J. Am. Chem. Soc. 2015, 137, 8696−8699

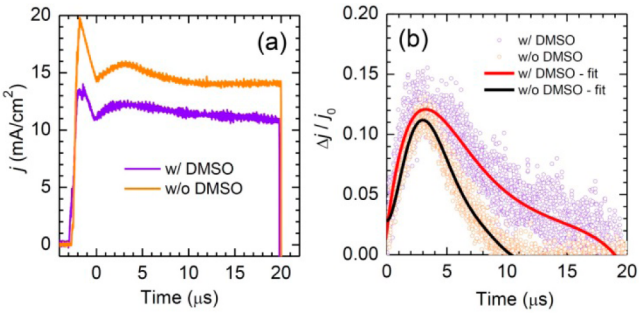

Figure 3. (a) Photo-CELIV current transients of perovskite solar cell consist of FTO/bl-Al_2O_3/mp-TiO_2/$MAPbI_3$/spiro-MeOTAD/Ag with DMF or DMSO/DMF used as solvents for $MAPbI_3$. (b) Current peaks (Δj) of photo-CELIV current transients normalized by their displacement current of capacitance (j_0), respectively. Curves were fitted by polynomial fitting to compare charge extraction behavior of sample with or without DMSO.

capacitance (j_0).[19,20] The difference in current density arises from difference in film thickness of 650 nm for the adduct-induced $MAPbI_3$ and 500 nm for the $MAPbI_3$ without DMSO because j_0 is defined as $j_0 = \varepsilon\varepsilon_0 A/d$ (ε, dielectric constant; ε_0, vacuum permittivity; A, voltage increase rate; d, film thickness).[19] The difference in film thickness at the given coating condition is attributed to change in viscosity by DMSO, which affect j_0 and entire current density. The charge carrier mobility is calculated by the equation with the current density at maximum peak (Δj) and t_{max} that is the time when the current density is maximized (see the details of the calculation in the Supporting Information).[20] The charge carrier mobility for the adduct-induced $MAPbI_3$ is estimated to be 3.9×10^{-3} $cm^2/(V\,s)$, which is slightly higher than 2.7×10^{-3} $cm^2/(V\,s)$ for the adduct free case (Table S1). Our sample shows one order of magnitude higher than the MACl-assisted one-step solution growth of $MAPbI_3$ (3.2×10^{-4} $cm^2/(V\,s)$).[21] In Figure 3b, Δj is normalized by j_0 to compare charge extraction behavior. Extracted charge is proportional to the area of the curve. Extracted charges of the adduct-induced $MAPbI_3$ are greater than those of the sample without DMSO. The extent of the extracted charges can explain charge recombination. Photoexcited electrons and holes will be extracted by built-in electric field or recombined in the absence of external electric field. Since photo-CELIV is designed to extract charges not by built-in electric field,[22,23] the extracted charges in Figure 3b result from the charges that are not recombined. Therefore, the more extracted charges in the adduct-induced $MAPbI_3$ is indicative of slow recombination.[10]

Figure 4 shows photovoltaic performance along with SEM images of the surface of $MAPbI_3$ and the cross-sectional full cell. The adduct-induced $MAPbI_3$ shows high dense nature with grains sizing from 200 to 300 nm (Figure 4a). As can be seen in FIB-assisted SEM images for the full cell with FTO/bl-TiO_2/mp-TiO_2/$MAPbI_3$/spiro-MeOTAD/Ag configuration in Figure 4b, highly dense $MAPbI_3$ film with plateau surface is constructed via adduct approach, where ca. 400 nm-thick capping layer is formed on the 230 nm-thick mp-TiO_2 film. The bl-TiO_2 layer and spiro-MeOTAD layer are about 40 and 190 nm, respectively.

We have tested several solvents except for diethyl ether, but diethyl ether is eventually found to be superior to other solvents in terms of reproducibility. The basis for relatively low reproducibility by other solvents such as toluene or chlorobenzene is because $MAPbI_3$ quality is significantly dependent on dripping amount and/or spinning rate of washing solvent, and

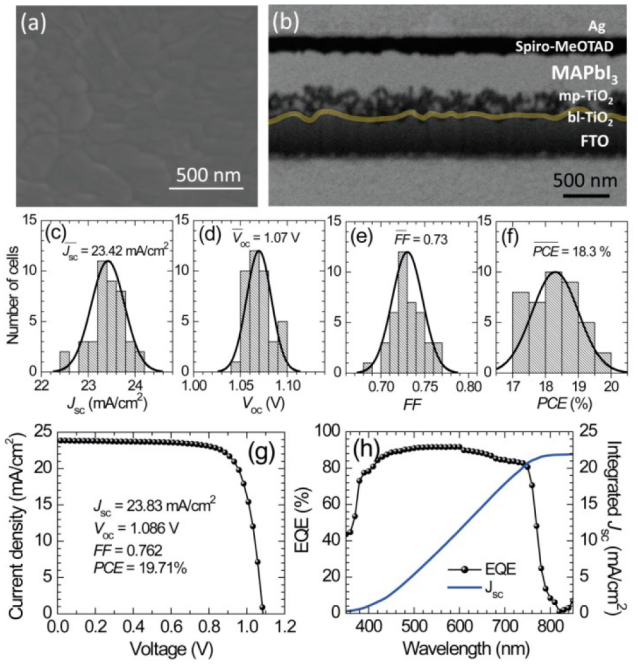

Figure 4. (a) Plan-view SEM image of $CH_3NH_3PbI_3$ and (b) FIB-assisted cross sectional SEM image of full cell structure of perovskite solar cell based on the adduct-induced $MAPbI_3$. The thickness of bl-TiO_2, mp-TiO_2, $MAPbI_3$, spiro-MeOTAD, and Ag were 40, 200, 400, 200, and 180 nm, respectively. (c–f) Histograms of short-circuit current density (J_{sc}), open-circuit voltage (V_{oc}), fill factor (FF), and power conversion efficiency (PCE) of 41 cells, respectively. (g) J–V curve and (h) external quantum efficiency (EQE) spectrum together with EQE date-based integrated J_{sc} for the best performing perovskite solar cell. J–V data were collected at reverse scan under AM 1.5G one sun illumination (100 mW/cm^2). The aperture mask area was 0.125 cm^2. The data were collected with the 16 h-aged cells because Ag electrode-based device showed normally poor fill factor right after fabrication.

difference in solubility between the solvent for washing and the solvent in the precursor solution. Highly reproducible $MAPbI_3$ films have been obtained using diethyl ether regardless of spin coating condition if one uses enough amount of diethyl ether for dissolving DMF completely. Photovoltaic parameters are gathered from 41 cells and statistically analyzed (Table S2). As can be seen in Figure 4c–f, the adduct-induced $MAPbI_3$ exhibits photovoltaic parameters with small standard deviation, leading to average short-circuit photocurrent density (J_{sc}) of 23.44 ± 0.37 mA/cm^2, open-circuit voltage (V_{oc}) of 1.070 ± 0.013 V, fill factor (FF) of 0.729 ± 0.019, and PCE of 18.30 ± 0.71%. The best PCE of 19.71% was achieved with J_{sc} of 23.83 mA/cm^2, V_{oc} of 1.086, and FF of 0.762 (Figure 4g). The measured J_{sc} is well consistent with the integrated J_{sc} of 22 mA/cm^2 estimated from IPCE in Figure 4h. It is noted that maximum IPCE reaches over 91%, which is mainly due to high charge extraction property of the adduct-induced $MAPbI_3$ and in part due to light reflection by the back Ag electrode. The high photocurrent density approaching 24 mA/cm^2 is confirmed not to exceed the theoretical maximum value of 26 mA/cm^2 as estimated by assuming 100% internal quantum efficiency and 5% optical loss from the FTO glass (Figure S3). J–V hysteresis is checked, and little hysteresis is found at slow scan rate, where PCE = 18.62% at reverse scan and 18.18% at forward scan showing 2% difference (Figure S4 and Table S3). The stabilized PCE is demonstrated by holding the

DOI: 10.1021/jacs.5b04930
J. Am. Chem. Soc. 2015, 137, 8696–8699

voltage at the maximum power point at a slow scan according to method described elsewhere (Figure S4).[24]

In conclusion, highly reproducible pervoksite solar cells were fabricated via Lewis base adduct of PbI_2. A 1:1:1 adduct of MAI·PbI_2·DMSO was formed by spin-coating of the DMF solution containing equimolar MAI, PbI_2, and DMSO and using diethyl ether to remove solvent DMF only. We achieved average PCE of 18.3% and best PCE of 19.7% by the adduct chemistry. Studies on materials, device structures, and chemical engineering of interfaces are expected to further improve the solar cell efficiency using the adduct-induced perovskite light absorber.

■ ASSOCIATED CONTENT

Supporting Information

Experimental details and characterization data. The Supporting Information is available free of charge on the ACS Publications website at DOI: 10.1021/jacs.5b04930.

■ AUTHOR INFORMATION

Corresponding Authors

*mchoi@snu.ac.kr

*npark@skku.edu

Author Contributions

§These authors contributed equally to this work.

Notes

The authors declare no competing financial interest.

■ ACKNOWLEDGMENTS

This work was supported by the Global Frontier R&D Program on Center for Multiscale Energy System funded by the National Research Foundation under the Ministry of Science, ICT & Future Planning, Korea (under contracts No. NRF-2011-0031561, NRF-2012M3A6A7054855, and NRF-2012M3A6A7054861).

■ REFERENCES

(1) Kim, H.-S.; Lee, C.-R.; Im, J.-H.; Lee, K.-B.; Moehl, T.; Marchioro, A.; Moon, S.-J.; Humphry-Baker, R.; Yum, J.-H.; Moser, J. E.; Grätzel, M.; Park, N.-G. *Sci. Rep.* **2012**, *2*, 591.

(2) Kojima, A.; Teshima, K.; Shirai, Y.; Miyasaka, T. *J. Am. Chem. Soc.* **2009**, *131*, 6050.

(3) Im, J.-H.; Lee, C.-R.; Lee, J.-W.; Park, S.-W.; Park, N.-G. *Nanoscale* **2011**, *3*, 4088.

(4) Liu, M.; Johnston, M. B.; Snaith, H. J. *Nature* **2013**, *501*, 395.

(5) Zhou, H.; Chen, Q.; Li, G.; Luo, S.; Song, T.-b.; Duan, H.-S.; Hong, Z.; You, J.; Liu, Y.; Yang, Y. *Science* **2014**, *345*, 542.

(6) Heo, J. H.; Han, H. J.; Kim, D.; Ahn, T. K.; Im, S. H. *Energy Environ. Sci.* **2015**, *8*, 1602.

(7) Jeon, N. J.; Noh, J. H.; Yang, W. S.; Kim, Y. C.; Ryu, S.; Seo, J.; Seok, S. I. *Nature* **2015**, *517*, 476.

(8) Yang, W.-S; Noh, J. H.; Jeon, N. J.; Kim, Y. C.; Ryu, S.; Seo, J.; Seok, S. I. *Science* **2015**, *348*, 1234.

(9) Burschka, J.; Pellet, N.; Moon, S.-J.; Humphry-Baker, R.; Gao, P.; Nazeerudin, M. K.; Grätzel, M. *Nature* **2013**, *499*, 316.

(10) Im, J.-H.; Jang, I.-H.; Pellet, N.; Grätzel, M.; Park, N.-G. *Nat. Nanotechnol.* **2014**, *9*, 927.

(11) Im, J.-H.; Kim, H.-S.; Park, N.-G. *APL Mater.* **2014**, *2*, 081510.

(12) Jeon, N. J.; Noh, J. H.; Kim, Y. C.; Yang, W. S.; Ryu, S.; Seok, S. I. *Nat. Mater.* **2014**, *13*, 897.

(13) Wharf, I.; Gramstad, T.; Makihja, R.; Onyszchuk, M. *Can. J. Chem.* **1976**, *54*, 3430.

(14) Reichardt, C. *Solvents and Solvent Effects in Organic Chemistry*, 3rd ed.; Wiley-VCH Publishers: Berlin, Germany, 2003.

(15) Pavia, D. L.; Lampman, P.; Kriz, G. S.; Vyvyan, J. R. *Introduction to Spectroscopy*; Brooks/Cole Press: Independence, KY, 2009.

(16) Colthup, N. B.; Daly, L. H.; Wiberley, S. E. *Introduction to Infrared and Raman Spectroscopy*, 2nd ed.; Elsevier: New York, 2012.

(17) Xiao, M.; Huang, F.; Huang, W.; Yasmina, D.; Zhu, Ye.; Etheridge, J.; Gray-Weale, A.; Bach, U.; Cheng, Y.-B.; Spiccia, L. *Angew. Chem.* **2014**, *126*, 10056.

(18) Miyamae, H.; Numahata, Y.; Nagata, M. *Chem. Lett.* **1980**, 663.

(19) Juška, G.; Arlauskas, K.; Viliūnas, M.; Kočka, J. *Phys. Rev. Lett.* **2000**, *84*, 4946.

(20) Juška, G.; Nekrašas, N.; Genevičius, K.; Stuchlik, J.; Kočka. *Thin Solid Films* **2004**, *451*, 290.

(21) Chen, Y.; Peng, J.; Su, D.; Chen, X.; Liang, Z. *ACS Appl. Mater. Interfaces* **2015**, *7*, 4471.

(22) Dennler, G.; Mozer, A. J.; Juška, G.; Pivrikas, A.; Österbacka, R.; Fuchsbauer, A.; Sariciftci, N. S. *Org. Electron.* **2006**, *7*, 229.

(23) Armin, A.; Velusamy, M.; Burn, P. L.; Meredith, P.; Pivrikas, A. *Appl. Phys. Lett.* **2012**, *101*, 083306.

(24) Christians, J. A.; Manser, J. S.; Kamat, P. V. *J. Phys. Chem. Lett.* **2015**, *6*, 852.

DOI: 10.1021/jacs.5b04930
J. Am. Chem. Soc. 2015, 137, 8696−8699